ORIGINAL RESEARCH

Carbonized cotton fabric-based multilayer piezoresistive pressure sensors

Lin Zhang · Hongqiang Li · Xuejun Lai · Tianyuan Gao · Xiaofeng Liao · Wanjuan Chen · Xingrong Zeng

Abstract Piezoresistive pressure sensors have attracted much attention for their potential applications in health monitoring, wearable devices, electronic skin and smart robots. Herein, we report an innovative strategy to fabricate multilayer piezoresistive pressure sensors with polydimethylsiloxane anchored carbonized cotton fabric (PACCF). Due to the good conductivity of carbonized cotton fabric and the multilayer structure to construct three-dimensional conductive network, the sensor possessed not only a wide pressure detection range, but also an ultrahigh sensitivity of 13.89 kPa^{-1} (0–6 kPa). Moreover, the sensor also exhibited fast response and excellent repeatability even after 500 loading–unloading cycles. Importantly, the sensor was successfully applied for detecting pulses, airflow, weak vibration and various body motions. Additionally, the sensors integrated sensing matrix also realized mapping and identifying spatial pressure distribution. Our method to fabricate PACCF-based multilayer piezoresistive pressure sensor is simple, efficient and low-cost; no special equipment or chemicals is required, and cotton as main raw material is natural and renewable, which is very beneficial for large-scale production. Our findings conceivably stand out as a new tool to fabricate high-performance pressure sensors in the fields of healthcare and emerging intelligent electronics.

L. Zhang · H. Li (✉) · X. Lai · T. Gao ·
X. Liao · X. Zeng (✉)
School of Materials Science and Engineering, Key Lab of Guangdong Province for High Property and Functional Polymer Materials, South China University of Technology, Guangzhou 510640, People's Republic of China
e-mail: lihq@scut.edu.cn

X. Zeng
e-mail: psxrzeng@gmail.com

W. Chen
College of Materials Science and Energy Engineering, Foshan University, Foshan 528000, People's Republic of China

Graphical abstract
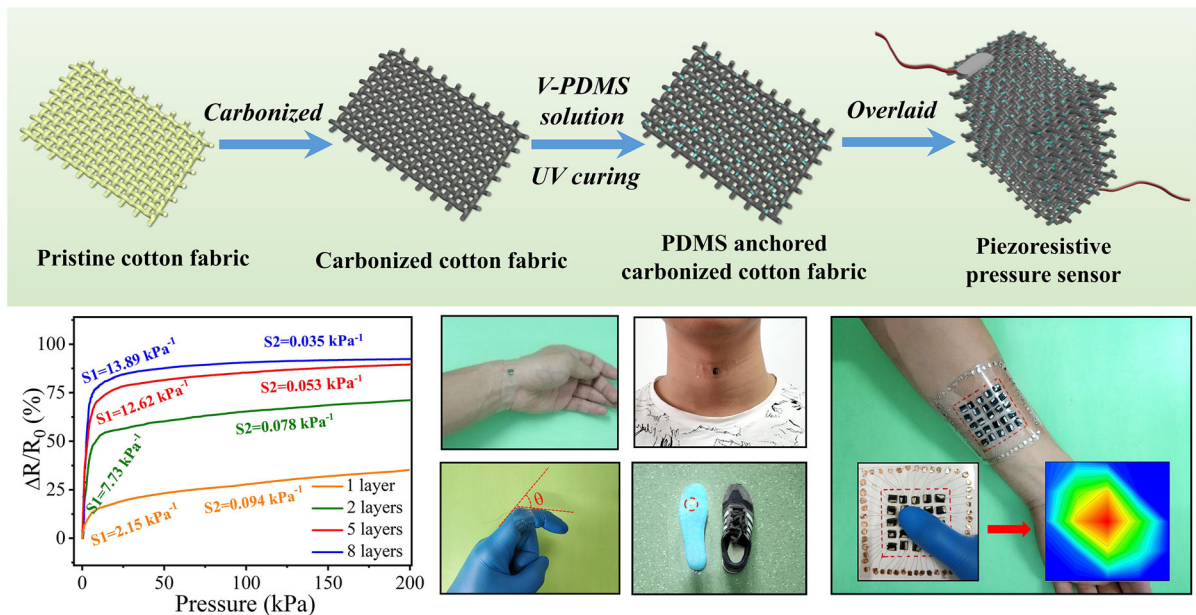
Introduction

Piezoresistive pressure sensors with the function of real-timely converting pressures into electrical signals have attracted enormous interest in the last decade, for potential industrial applications in healthcare (Lou et al. 2016), interactive wearable devices (Lee et al. 2015), electrical skin (Kim et al. 2011; Lou et al. 2017), smart robots (Viry et al. 2014), and so forth. Generally speaking, the conductive sensing materials are considered to be essential for constructing conductive pathways of pressure sensors under exterior pressure. However, the conventional conductive materials including semiconductors and metal foils are rigid and low-resolution, and unable to fulfill the requirements of wearable pressure sensors. In recent years, various conductive sensing materials such as electrically conductive polymers (Yang et al. 2018a; Zhong et al. 2016), metal nanowires (Wei et al. 2015; Xu et al. 2017), carbon nanotubes (Xiang et al. 2018; Liang et al. 2018; Su et al. 2018) and graphene sheets

(Wang et al. 2018; Gao et al. 2013; Wan et al. 2014) (containing various reduced graphite oxide) were utilized to ameliorate the sensitivity, detection range, flexibility and other performances of the pressure sensors. For example, Chun et al. (2015) prepared a highly sensitive pressure sensor with a double-layered graphene obtained by thermal chemical vapor deposition (CVD) (Chun et al. 2015). Gong, et al. (2014) reported a high-sensitivity and fast-response pressure sensor with ultrathin gold nanowires. Nevertheless, considering the limitations such as high cost and complicated fabrication process, it is difficult to meet the requirements of the sensors in large-scale practical applications. Recently, Deng et al. (2017) and Zhang et al. (2017) both proposed the new strategy to prepare sensor with low-cost carbonized cotton fabric (CCF) in the presence of flexible polydimethylsilane (PDMS) (Deng et al. 2017; Zhang et al. 2017), while the single conductive CCF layer limited the sensitivity of sensors.

The microstructure is also critical for the performance especially sensitivity of piezoresistive pressure sensors especially under a low pressure. To achieve excellent sensitivity, the sensing materials with various interlocking rough surface or ingenious array microstructures were constructed for pressure sensors (Zhong et al. 2016; He et al. 2015; Choong et al. 2014;

Pang et al. 2012; Wu et al. 2016). For example, by introducing three-scale nested microstructures on polypyrrole film, Yang et al. (2018a) fabricated a sensor with a high sensitivity up to 19.32 kPa^{-1} in the pressure range of 0–2 kPa. Park et al. (2014) also prepared a high-sensitivity sensor based on carbon nanotubes/polydimethylsiloxane (CNTs/PDMS) composite films with microdome arrays. In addition, Ma et al. (2018) reported the preparation of 3D microporous conductive elastomer coated with synergistic multiwalled CNTs and graphene for pressure sensor. However, the construction processes for the microstructures were complicated and time-consuming, and special equipment was usually required. Moreover, due to the small reversible deformations of the microstructures, the sensors only appeared high sensitivity under low pressure. In the case of high pressures generated by mobile blood, object manipulation, and some vigorous exercises such as jumping and running, the microstructures were easily to be saturated, thus leading to the ineffectiveness of the sensors. Therefore, it is a significant value to simultaneously realize high sensitivity and wide pressure range of piezoresistive pressure sensors toward further expanding their applications.

Herein, we propose a new method to fabricate wide-range and high-sensitivity multilayer piezoresistive pressure sensor. It was based on the utilization of carbonized cotton fabric (CCF) with air-gap microstructure to endow superior conductivity and further UV-curing of polydimethylsiloxane (PDMS) to anchor carbonized cotton fabric for improving flexibility and resilience. By stacking the PDMS anchored CCF (PACCF), the piezoresistive pressure sensor with multilayer structure was easily obtained. The chemical structure of the PACCF was characterized by X-ray diffraction (XRD) and Fourier transform infrared (FT-IR) spectroscopy, and the relation between layer number and piezoresistive performance of the sensor was investigated. The sensor achieved not only a wide working range of 0–200 kPa but also an ultrahigh sensitivity of 13.89 kPa^{-1} in the range of 0–6 kPa. Moreover, the sensor also exhibited fast response and excellent repeatability. Importantly, the sensor was successfully applied for detecting various behaviors such as pulse, airflow, weak vibration and body motions, and the sensors integrated sensing matrix could be used to map and identify spatial pressure distribution. Our findings illustrate a new strategy to fabricate high-performance pressure sensors for health monitoring, wearable devices, artificial intelligence, electronic skin and other special application scenarios.

Materials

Vinyl-terminated polydimethylsiloxane (V-PDMS, average MW = 6000) was supplied by Meryer (Shanghai) Chemical Technology Co., Ltd. (China). Trimethylolpropane triacrylate (TMPTA, 85%), 2-hydroxy-2-methylproplophenone (Darocur 1173, 97%) and hexane were provided by Aladdin Reagent Co., Ltd. (China). Cotton fabrics (Plain weave, 79.6 g/m^2, yarn count of 100 Nm and warp of 40 yarn/cm and weft of 40 yarn/cm) were bought from local stores. All chemicals were used as received without further purification.

Fabrication of PACCF-based multilayer piezoresistive pressure sensors

The carbonized cotton fabric (CCF, 3 cm × 3 cm) was firstly prepared at high temperature (see supporting information) and then immersed in V-PDMS solutions containing 1.25 g of V-PDMS, 0.125 g of TMPTA, 0.02 g of Darocur 1173 and 25 g of hexane for 1 min. Subsequently, both sides of the taken-out CCF were respectively exposed under UV light (INTELLI-RAY 400, Uvitron International, Inc., USA) for 2 min with a distance of 15 cm between the samples and the center of UV light lamp and then dried at 60 °C for 1 h to obtain PDMS anchored CCF (PACCF).

To fabricate five-layer piezoresistive pressure sensor, five pieces of PACCF (0.5 cm × 0.5 cm) were stacked, and the top and bottom layers were respectively connected with a fine copper wire (diameter = 0.1 mm) as electrodes covered with a small amount of silver paste to ensure the flatness of the joint surface. After that, two pieces of polyvinyl chloride (PVC) plate (0.5 cm × 0.5 cm × 0.2 mm) were fixed on the top and bottom layers by 3 M Scotch transparent tape (600-HC33), and the five-layer piezoresistive pressure sensor was obtained. The schematic illustration for the fabrication process of five-layer pressure sensor is presented in Fig. 1. For comparison, one-layer, two-layer and eight-layer piezoresistive
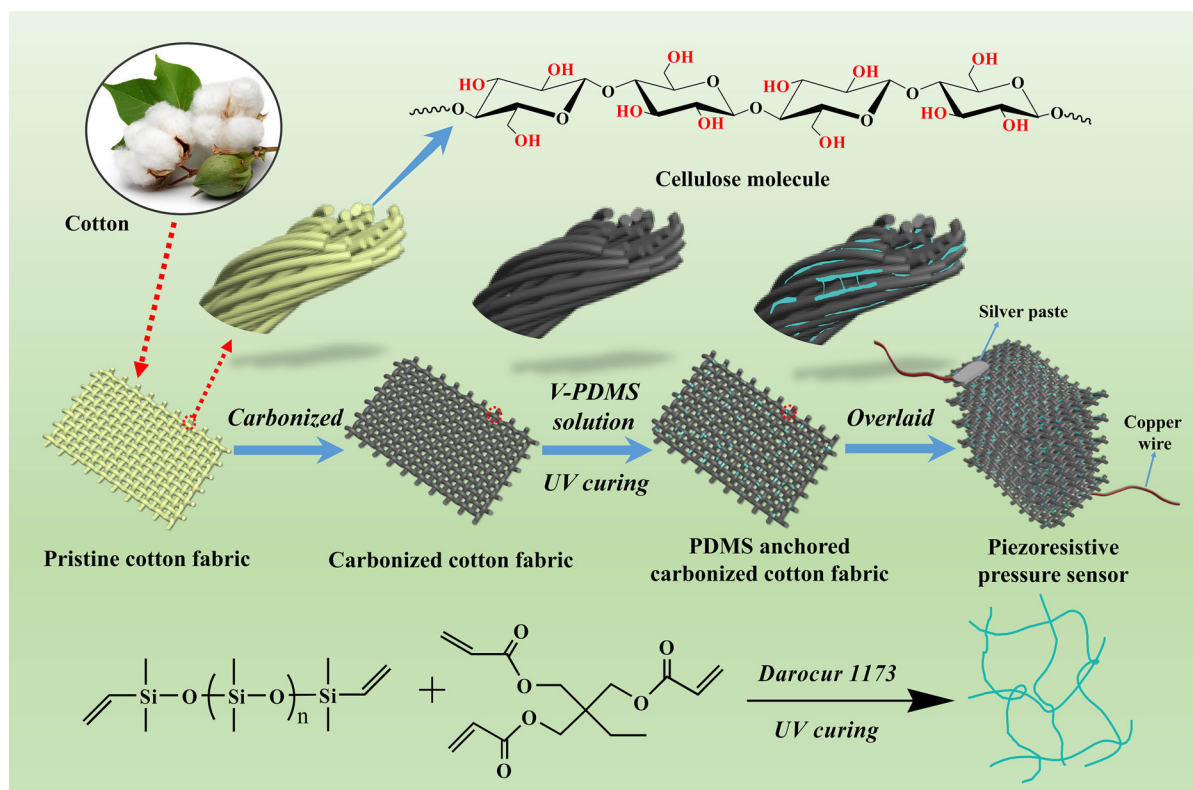
Fig. 1 Schematic illustration for the fabrication process of PACCF-based five-layer piezoresistive pressure sensor

pressure sensors were also respectively fabricated with different pieces of PACCF.

Characterizations

Fourier transform infrared spectroscopy (FT-IR)

FT-IR spectra were carried out on a Tensor 27 spectrometer (Bruker Optics, Germany) using attenuated total reflectance (ATR) mode from 4000 to 600 cm^{-1} with a resolution of 4 cm^{-1}.

Scanning electron microscopy (SEM)

SEM was conducted on a field emission scanning electron microscope (Merlin, Carl Zeiss Jena, Germany) at an acceleration voltage of 5.0 kV.

Raman spectroscopy

Raman spectrum was collected on a LabRAM ARAMIS Raman confocal microscope (532 nm,

Aramis CRM, Horiba Jobin–Yvon, Edison, NJ) from 400 to 4000 cm^{-1}.

X-ray diffractometer (XRD)

XRD spectra were recorded on a Bruker D8 Advance Diffractometer (Bruker, Germany) using Cu Kα radiation source ($\lambda_1 = 1.54060$ Å, $\lambda_2 = 1.54439$ Å) and a LynxEye_XE detector.

Sheet resistance

Sheet resistances of CCF and PACCF were performed on a four-point probe resistance measurement system (RTS-9, Four Probe Tech., Guangzhou).

Piezoresistive performances

The piezoresistive performances of the PACCF-based pressure sensors were measured with an all-electric dynamic test instrument (ElectroPuls E1000, Instron, USA) and a semiconductor characterization system

(Keithley 4200-SCS, USA) at a constant bias voltage of 5 V (see Fig. S1). The tester for various applications is a 26-year-old healthy male with a weight of 78 kg and a height of 180 cm.

Sensitivity calculation

The sensitivity (S) of the piezoresistive pressure sensors was calculated according to the following equation (Chen et al. 2018),

$$S = \frac{(\Delta R/R_0) \times 100\%}{\Delta P}$$

where R_0 was the initial resistance of the pressure sensor without applied pressure, ΔR referred to the relative changes of resistance and ΔP represented the change of the applied pressure. Here, the sensitivities in the low pressure range (0–6 kPa) and the high pressure range (20–200 kPa) were defined as S1 and S2, respectively.

Results and discussion

Preparation and structural characterization of PACCF

The carbon-based materials from natural biomaterials such as cotton and silk have attracted extensive research interests in the field of sensors owing to their excellent electrical conductivity, low cost and environmental benignity (Wang et al. 2017; Zhang et al. 2017). In this work, after a simple high-temperature carbonization treatment, the commercially available cotton fabric was endowed with high conductivity, while still maintaining the original integrity and flexibility of the fibers (Hao et al. 2018). To further improve the flexibility and resistance to exterior force, the carbonized cotton fabric (CCF) was immersed in PDMS solution containing crosslinker and photoinitiator and then exposed under UV light to form crosslinked organosilicon on the carbonized fibers to play the anchoring role. The microscopic morphologies of pristine CF, CCF and PDMS anchored CCF (PACCF) were observed by SEM as shown in Fig. 2. It was obvious to note that the pristine CF was composed of warp and weft yarns (each yarn including dozens of twisting cotton fibers) aligned to form simple crisscross patterns. In comparison, the CCF had more

intersections at the same magnification (50×). It was consistent with the fact that the actual surface area and weight respectively shrank by 47.3% and 83.2% after annealing. Furthermore, the CCF possessed high conductivity with a sheet resistance of 276 Ω/sq. As can be seen from the magnified images (200× and 1000×), the dimension of air gaps between the thinner carbonized fibers obviously became wider. It was very beneficial for the piezoresistive pressure sensor to achieve high sensitivity (Liu et al. 2018; Tao et al. 2017). From the images of PACCF, the crosslinked PDMS was observed to be randomly and partly covered on the carbonized fibers, which could effectively improve the flexibility of the CCF by anchoring the fibers. Additionally, the crosslinked PDMS had little effect on the electrical conductivity of CCF, and the sheet resistance of PACCF only slightly increased to 293 Ω/sq.

To further study the chemical structure of different fabrics, Raman, FT-IR and XRD spectra were respectively carried out and the results are presented in Fig. 3. In the Raman spectrum (Fig. 3a), two characteristic bands of D-band (defect-induced band) peak at ∼ 1344 cm^{-1} and G-band (crystalline graphite band) peak at ∼ 1604 cm^{-1} were observed, demonstrating the amorphous structure of CCF (Li et al. 2016). From the FT-IR spectrum of pristine CF (Fig. 3b), a wide stretching peak of -OH around 3320 cm^{-1}, the bending vibration peak of hydrocarbon structures at 1312 cm^{-1} and the symmetric stretching peaks of carboxylate groups at 1367 and 1426 cm^{-1} appeared, which were all originated from cellulosic molecules (Lin et al. 2018). After high-temperature carbonization, the characteristic peaks all disappeared as shown in the FT-IR spectrum of CCF. Furthermore, as can be seen from the FT-IR of PACCF, the new peaks around 2900 cm^{-1} were attributed to the stretching vibration of –CH$_3$ and –CH$_2$– groups, and the characteristic peaks of Si–O bonds were observed in the range of 1100–790 cm^{-1} (Su et al. 2017). In addition, the XRD pattern of CCF in Fig. 3c showed two broad peaks at 28° and 43°, respectively corresponding to the crystallographic planes of (002) and (100) in the disordered carbon structure (Li et al. 2016; Zhao et al. 2007). Obviously, the pattern of PACCF was not affected by the small amount of the crosslinked PDMS, and similar to that of CCF.
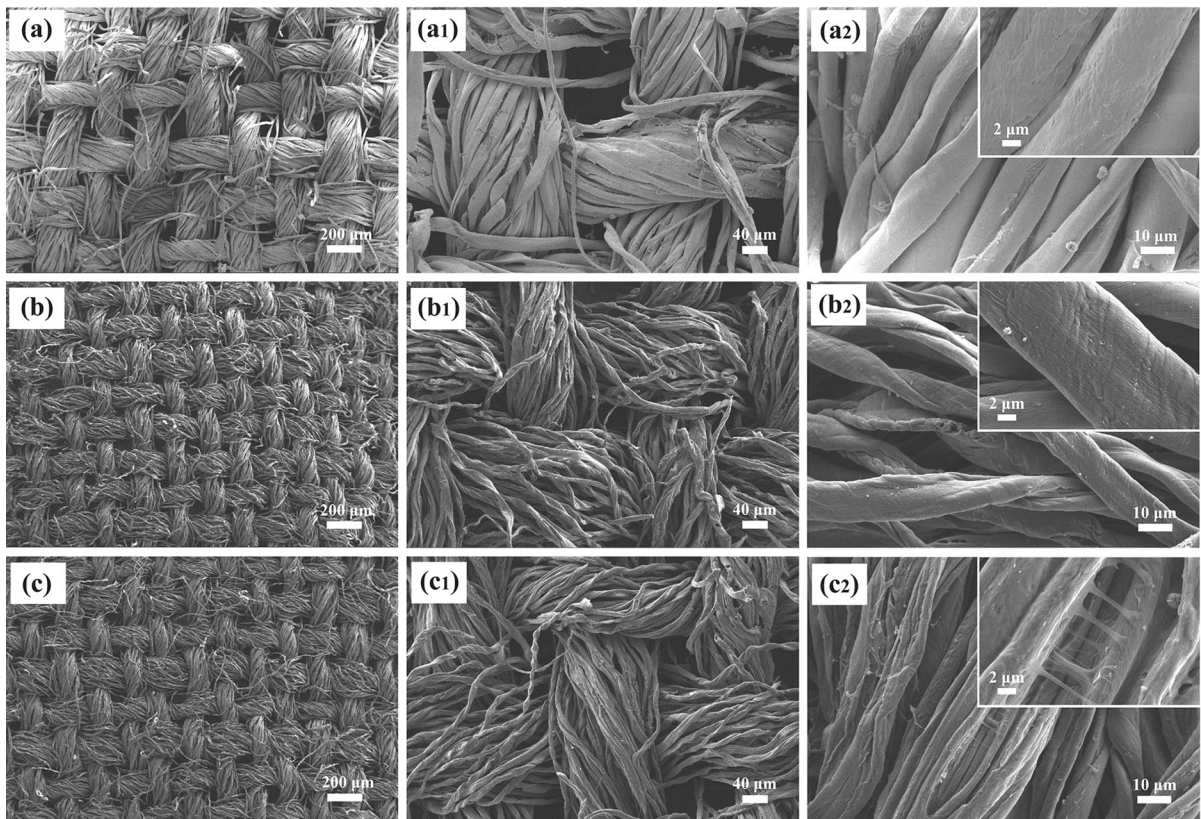
Fig. 2 SEM images of **a** pristine CF, **b** CCF and **c** PACCF at 50×, and the corresponding SEM images with higher magnifications at 200× **a1**, **b1**, **c1**, 1000× **a2**, **b2**, **c2** and 5000× (inset on the top right)

Piezoresistive performances of PACCF-based piezoresistive pressure sensors

Clearly, the conductive PACCF with air-gap microstructure was very suitable for fabricating piezoresistive pressure sensors. However, the air spacings among the carbonized fibers of one-layer PACCF-based pressure sensor were limited. The number of the electrical pathways and the resistance only changed in a small range under exterior pressure, and the sensor was unable to achieve high sensitivity. Here, several pieces of PACCF were innovatively staked to fabricate mini-portable and three-dimensional sensor (see Fig. S2). Under pressure, the hierarchical air gaps among the carbonized fibers and the adjacent PACCF layers both decreased, leading to the obvious changes of the number of conductive pathways and the piezoresistive effect. A simple piezoresistive test was carried out with a five-layer piezoresistive pressure sensor. Firstly, the sensor

with a resistance of 2.15 kΩ was connected into a 6.5 V circuit, and 40 light-emitting diode (LED) lamps emitted a faint light. When put a 200 g weight on the sensor, the resistance quickly decreased to 0.27 kΩ, and the light of the LED lamps became more splendid. After removing the weight, the resistance recovered to 2.13 kΩ (see Fig. S3 and Video S1), showing obvious piezoresistive effect.

Figure 4a presented the effect of layer number on the resistance changes of the pressure sensors with pressure increasing. Obviously, as pressure increased, the sensitivities gradually decreased and exhibited two linear relationship intervals in a low pressure range of 0–6 kPa and a high pressure range of 20–200 kPa. It was also clear to note that the layer number had a large effect on the sensitivity of the sensors. The S1 and S2 of the single layer fabric were 2.15 kPa^{-1} and 0.094 kPa^{-1}, respectively. With the increase of the number of layers, the S1 remarkably increased and the S2 slightly decreased. The five-layer and eight-layer

Fig. 3 **a** Raman spectrum of the CCF; **b** FT-IR and **c** XRD spectra of pristine CF, CCF and PACCF
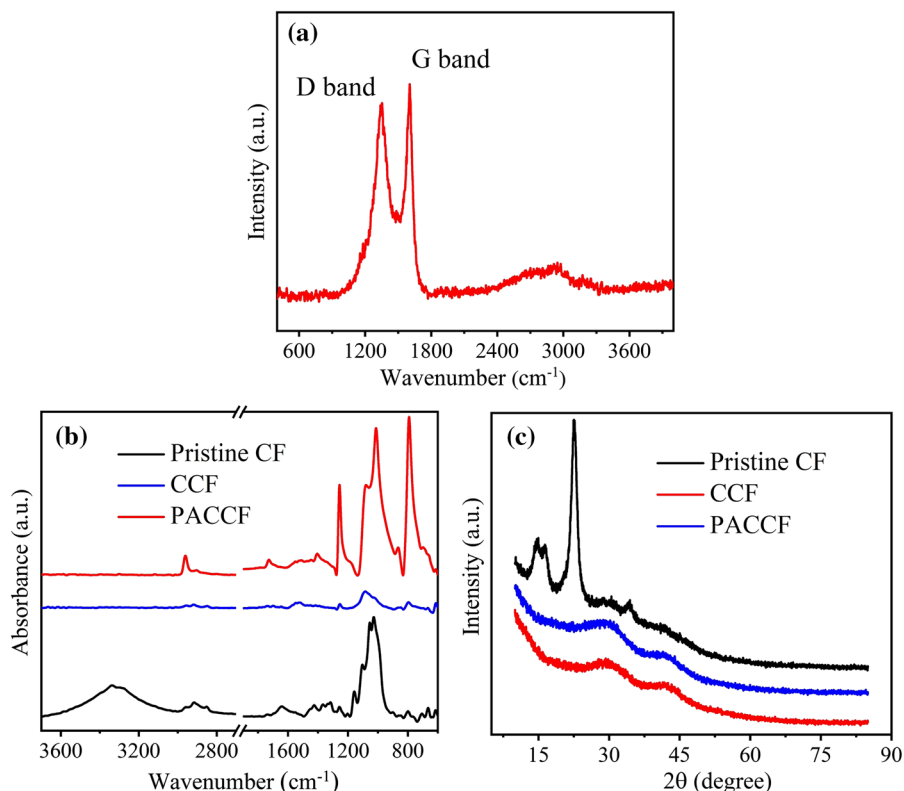
sensors had the high sensitivity of 12.62 and 13.89 kPa^{-1} in the low pressure range of 0–6 kPa, and still maintained at 0.053 and 0.035 kPa^{-1} in the high pressure range of 20–200 kPa, respectively. Moreover, the other two five-layer sensors prepared by the same procedure showed the similar sensitivities, no obvious difference was observed, demonstrating the good reproducibility of sensors (see Fig. S4). Compared with previously reported pressure sensors, PACCF-based multilayer pressure sensors realized not only an ultrahigh sensitivity but also a wide working range (see Table S1). Here, the five-layer sensor was chosen for the following various electrical performance tests and applications. Figure 4b shows the current–voltage (I–V) characteristics of the five-layer PACCF-based pressure sensor under the different pressures of 0, 4, 20 and 160 kPa. It can be seen that all the characteristic curves appeared a linear trend, demonstrating "Ohmic" behavior of the sensor under different pressures (Park et al. 2015). From the current values of the sensor at different pressures in Fig. 4c, it was obvious to note that the currents remained almost unchanged even after 1000 s, manifesting the good

electrical stability of the sensor (Konwar et al. 2017). In addition, the response and repeatability characteristics of the pressure sensor were studied under various pressures of 4, 8, 20, and 80 kPa, respectively. As shown in Fig. 4d, the sensor kept a stable response during five loading–unloading cycles under various pressures. Next, a test on the response time and relaxation time of the pressure sensor was performed and the results are presented in Fig. 4e, f. Under the pressure of 20 kPa, the response time and recovery time of the sensor attained about 64 and 165 ms, respectively. Moreover, the electrical cycling responses of the pressure sensor also had no frequency dependence in the range of 0.1–1 Hz (see Fig. S5). To further explore the stability of the sensor, we performed a repeatability testing of the pressure sensors for 500 loading–unloading cycles in the pressure range of 2–20 kPa (Fig. 4g). From the currents of the cycles in 90–100 and 400–410 s, the values were almost same, and no obvious difference was observed, indicating the excellent repeatability of the PACCF-based pressure sensor.
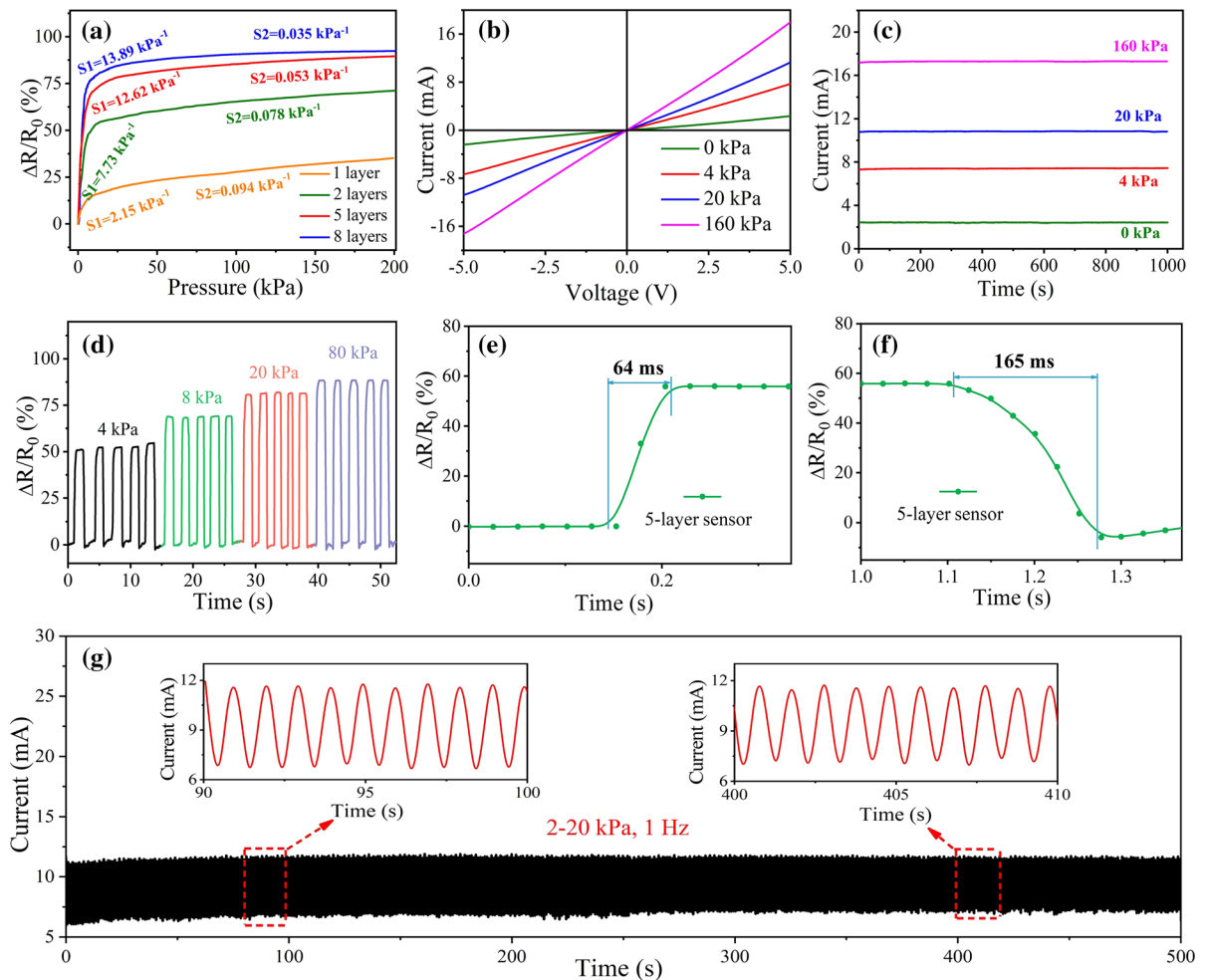
Fig. 4 a Resistance change of the sensors fabricated with one, two, five and eight layers of PACCF with pressure increasing; b I–V characteristics and c stability determination of the five-layer sensor; d Response test of five-layer sensor under different pressures. Response times of five-layer sensor for e loading and f unloading; g Repeatability performance of the five-layer sensor during 500 loading–unloading cycles in the pressure range of 2–20 kPa at frequency of 1 Hz, and the homologous enlarged image of 90–100 and 400–410 s

To understand the piezoresistive mechanism of the multilayer pressure sensors, we established the intuitionistic schematic models as shown in Fig. 5. When a small pressure was applied on one-layer pressure sensor, the number of the contact points inhering in conductive network constructed by carbonized fibers increased owing to the disappearance of the primary air spacing among the fibers. As pressure increased to a high value, the elastic deformation of the flexible fibers led to the further increase of the contact area and electrical pathways, thus resulting in the continuous decrease of the resistance. Differently, except the obvious increase of primary air spacing among the

carbonized fibers, the multilayer pressure sensors also had the secondary air spacing between the adjacent carbonized fabrics with rough corrugated surfaces. As a result, even under a low pressure, the spacing in multilayer pressure sensor drastically decreased and more electrical pathways were formed, leading to the sharp decline of resistance. Additionally, by virtue of the excellent flexibility and mechanical performance, the elastic deformations of the PDMS anchored carbonized fibers was reversible and sustainable, which could ensure the long-term application of the pressure sensor.
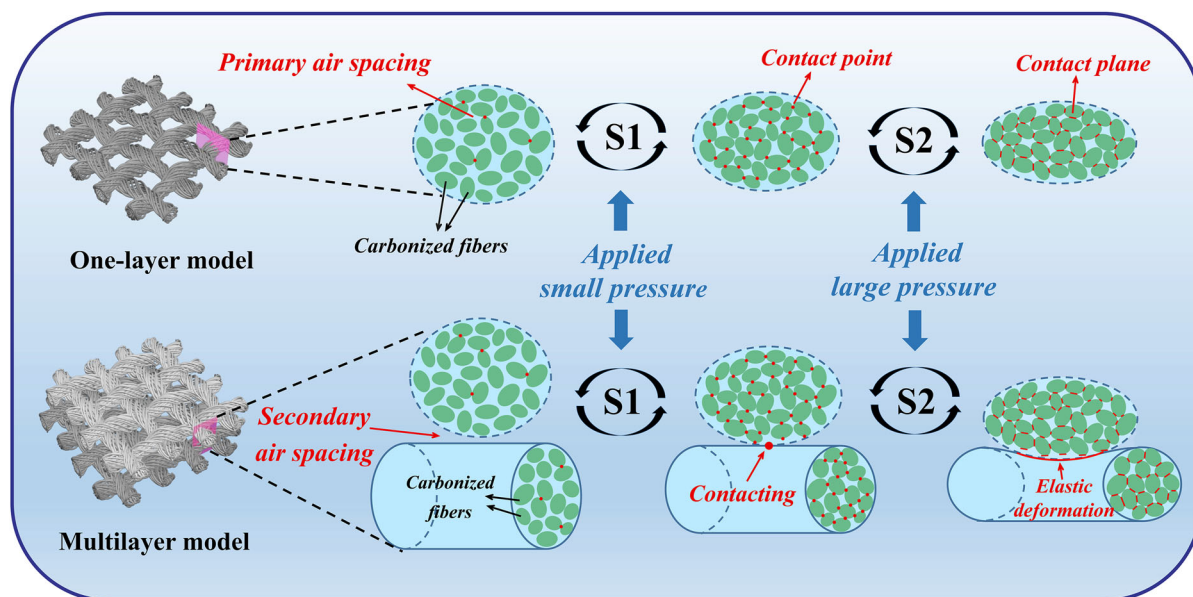
Fig. 5 Schematic models for the piezoresistive mechanism of one-layer and multilayer PACCF-based pressure sensors

Various applications of PACCF-based multilayer piezoresistive pressure sensor

As proof-of-concept examples, various scenes closely related to humans and daily life in which the multilayer piezoresistive pressure sensor participated were demonstrated. At first, the sensor was attached to a wrist band with tape for detecting real-time pulse signals under relaxation conditions (Fig. 6a, Video S2), and the real-time electrical current change lasting about 13 s was recorded in Fig. 6b. It was interesting to note that the pulse signals were repeatable and regular with an approximately frequency of 65 beats min^{-1}, which was close to the normal level of humans. As can be seen from the close-up of a single pulse peak in Fig. 6c, the typical characteristics of pulse waveforms including percussion wave (P-wave), tidal wave (T-wave) and diastolic wave (D-wave) were clearly observed (Yang et al. 2018b), which was very beneficial for the medical workers to real-timely monitor some paroxysmal diseases such as asthma and heart attack (Park et al. 2015). Figure 6d shows the changes in resistance of the sensor when being intermittently blew with a rubber ball. It can be seen that each airflow by the rubber ball was clearly corresponding to the peaks represented the increasing current in the signal curve, demonstrating the applicability of the sensor under small pressures even slight

airflow (Wang et al. 2015). In addition, the sensor was also attached at the throat of a tester as shown in Fig. 6e for recognizing the slight and complicated muscle movements induced by swallowing and speaking different words, and the corresponding signals are presented in Fig. 6f-h. Interestingly, the action of swallowing and the pronunciations of some words such as "Good" and "Work" could be distinctly recorded, and the corresponding signal waveforms exhibited good repeatability.

To further investigate the potential application, the five-layer piezoresistive pressure sensor was tightly attached on a Bluetooth speaker to detect the weak vibration stimuli (Wei et al. 2016) as shown in Fig. 7a. When the song "Try" played at a higher volume, the change in the rhythm of the music caused a series of changes in vibration amplitude, leading to the change of the pressure reflected in the curve of current signal in Fig. 7b. Obviously, when playing the song for the second time, the obtained signal curve was highly identical with the first one, showing good repeatability. After that, we also attached the sensor on the skin at the eye corner to detect the movements of the eyelids (Fig. 7c). With the repeated eye motions accompanying the muscle movements around the eyes such as looking up, closing and looking forward, the generated tiny pressure changes were accurately detected by the sensor, and a series of regular and
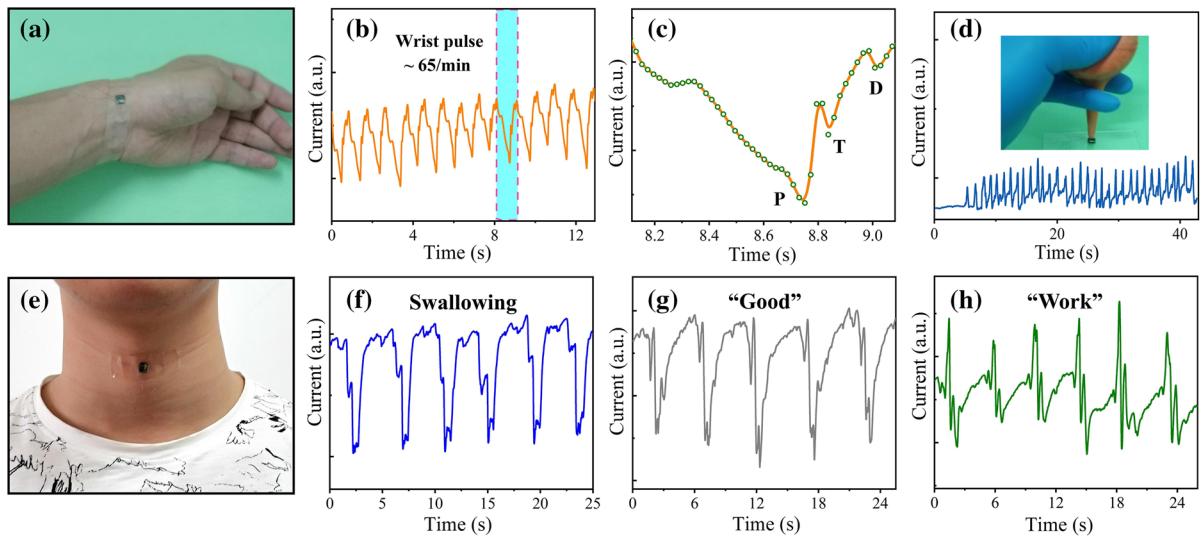
Fig. 6 a, **b** Real-time measurement of the pulse and the corresponding signal curves with the sensor mounted on the wrist; **c** enlarged view of the selected range from **b**; **d** real-time response curve of the sensor under the airflow from rubber ball; **e** The sensor pasted on the throat for recognizing the slight muscle movements. The response curves when the tester **f** took the motion of swallowing and **g**, **h** spoke "Good" and "Work", respectively
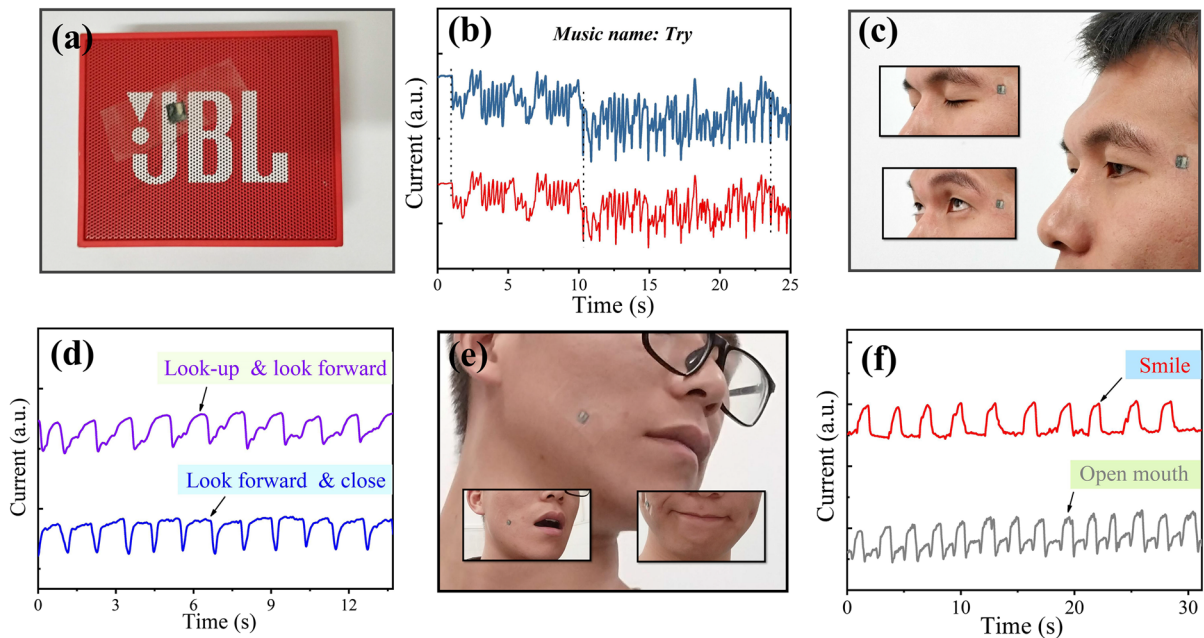

Fig. 7 a, **b** Detecting the sound-driven weak vibrations by attaching sensor on a Bluetooth speaker and the corresponding real-time recording of relative current; **c**, **d** Sensing results of visual angle variation by adhering the sensor on the eye corner; **e** Detecting facial expressions of smile and mouth motion by pasting sensor on the skin near the mouth; **f** Relative current changes when the tester smiled, opened and closed mouth, respectively

high identification variations of electrical current were outputted as shown in Fig. 7d. Furthermore, the sensor was pasted on the skin near the mouth to detect facial

expressions of smile as well as opening and closing mouth. As shown in Fig. 7e, f, when the face of the tester remained relaxing, the current was stable.

However, once the tester smiled or opened mouth, the sensor promptly outputted the corresponding signals in the current–time curves. When the tester repeated these motions, the signals showed the repetitive patterns, verifying the good stability of the sensor.

Except the low pressures, the sensor was also applied to respond to the higher pressures generated by the movements of finger and the flexions of wrist (Xia et al. 2018) as shown in Fig. 8a, d. It can be seen from Fig. 8b, e that the current appeared the quick and stable responses to the finger and wrist at different angles. Moreover, there was a cubic function relationship between relative resistance change ($\Delta R/R_0$) and bending angles (θ), as indicated by the fitting curves in Fig. 8c, f, showing the potential of the sensor in robot technology and other virtual realities. The sensor was

further placed on the knee and insole of the tester as shown in Fig. 8g, i to real-timely detect the motions such as walking and running. From Fig. 8h, j, the response waveforms corresponding to walking and running were regular, stable, repetitive, and easy to be distinguished. It was convenient for human to comprehensively monitor and evaluate the motion status, which was different from the ordinary function of Apple Watch to count step number. Therefore, the sensor can be utilized to detect not only the low pressures but also high pressures, showing the wide range in practical applications.

To imitate tactile sensing via e-skin, we designed and fabricated a large-area flexible sensor matrix of 25 pixels by integrating multiple sensors on a PET film for the detection of spatially resolved pressure (Cai
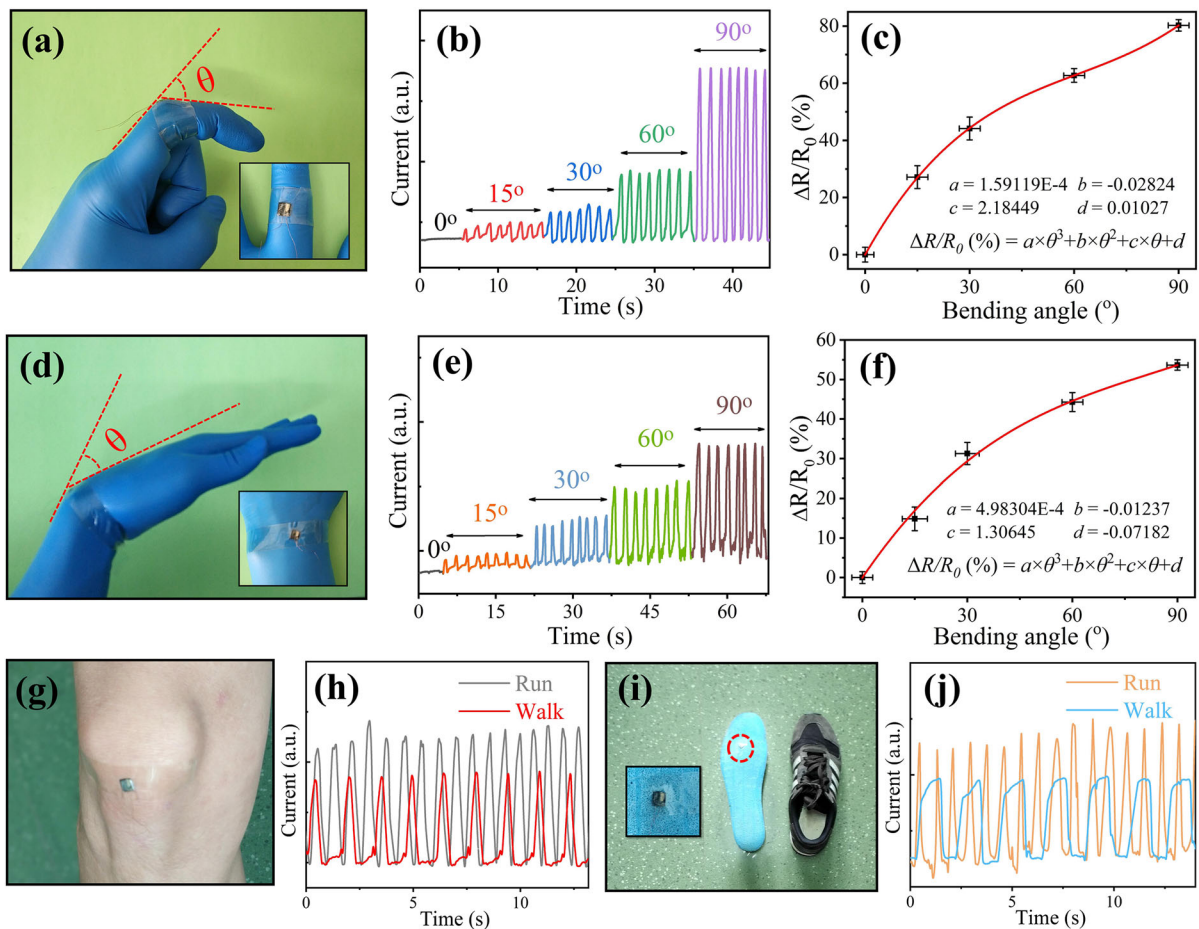

Fig. 8 Detection of **a**, **b** the second knuckle motions of index finger and **d**, **e** the wrist movements at different bending angles; The fitting curve and cubic function relationship of **c** index finger motions and **f** wrist movements between the relative resistance change ($\Delta R/R_0$) and bending angles (θ), respectively; The photographs and the corresponding response curves for the tester when walking and running by placing sensor on the knee **g**, **h** and insole **i**, **j**, respectively
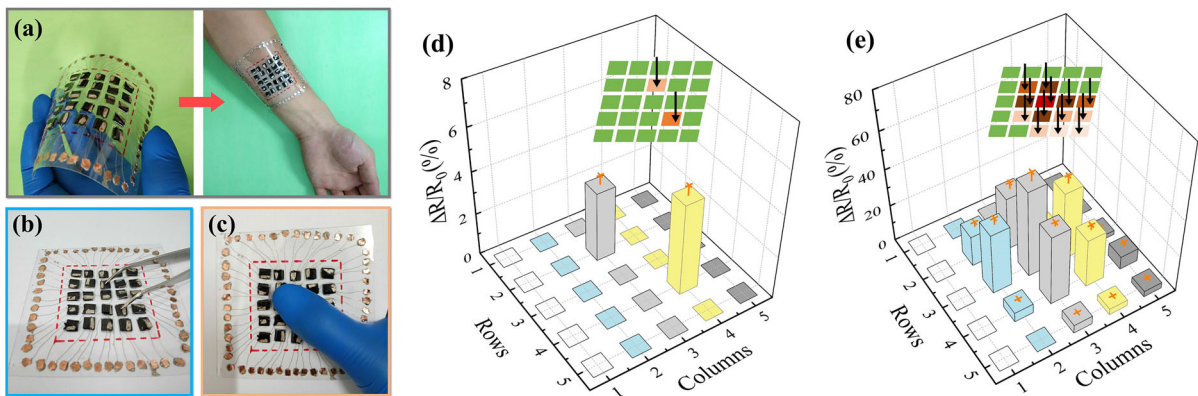
Fig. 9 a A wearable tactile-sensing integrated sensor matrix (5 × 5 elements) with multilayer piezoresistive pressure sensors; **b**, **c** Photographs of "Point" and "Plane" pressures applied with bent tweezers and thumb press, respectively; **d**, **e** The pressure distribution for "Point" and "Plane" stresses, respectively

et al. 2017; Liu et al. 2017), as shown in Fig. 9a. The pixelated sensor arrays can be attached on the human skin for monitoring all the signals of tactile sensing in the area. If exerting "Point" pressure with a metal bent tweezer on the matrix, the corresponding resistance changes of the local pixels could be easily detected, demonstrating the directional response of the integrated sensor matrix to external stimulation in a small local area (Fig. 9b, d). Differently, if exerting "Plane" pressure with a thumb as shown in Fig. 9c, the distribution of the applied pressure on the sensor matrix was detected, and the multidimensional tactile sensing image was successfully obtained as shown in Fig. 9e. Meanwhile, the corresponding resistance change mapping of the flexible sensor matrix sensor was also achieved (see Fig. S6), and the color contrast mapped the force distribution in consistency with the shape of thumb.

Conclusions

In summary, we demonstrated a novel method to fabricate carbonized cotton fabrics-based multilayer piezoresistive pressure sensor. Owing to the large number of air spacings in 3D conductive network and the excellent flexibility of the PDMS anchored carbonized fibers, the sensor possessed a wide pressure detection range of 0–200 kPa and high sensitivity up to 13.89 kPa^{-1} in 0–6 kPa. In addition, the response time and relaxation time of the sensor respectively reached 64 ms and 165 ms. After 500 loading–unloading cycles, the sensor still maintained excellent repeatability. Furthermore, the sensor was successfully applied to detect pulse, airflow, weak vibration and various body motions. Meanwhile, the large-area flexible sensor matrix integrated by the sensors was utilized for mapping and identifying spatial pressure distribution. The fabrication procedure is facile, efficient, cost-effective and available for large-scale production. Our results as proof-of-concept show the utilization of carbonized cotton fabrics to construct multilayer piezoresistive pressure sensors, exhibiting the great potential in the fields of healthcare, interactive wearable devices, electronic skin and smart robot.

Compliance with ethical standards

Conflict of interest All authors declare that they have no conflict of interest.

References

Cai Y, Shen J, Dai Z, Zang X, Dong Q, Guan G, Li LJ, Huang W, Dong X (2017) Extraordinarily stretchable all-carbon collaborative nanoarchitectures for epidermal sensors. Adv Mater 29:1606411

Chen Q, Cao PF, Advincula RC (2018) Mechanically robust, ultraelastic hierarchical foam with tunable properties via 3D printing. Adv Funct Mater 28:1800631

Choong CL, Shim MB, Lee BS, Jeon S, Ko DS, Kang TH, Bae J, Lee SH, Byun KE, Im J (2014) Highly stretchable resistive pressure sensors using a conductive elastomeric composite on a micropyramid array. Adv Mater 26:3451–3458

Chun S, Kim Y, Oh H-S, Bae G, Park W (2015) A highly sensitive pressure sensor using a double-layered graphene structure for tactile sensing. Nanoscale 7:11652–11659

Deng C, Pan L, Cui R, Li C, Qin J (2017) Wearable strain sensor made of carbonized cotton cloth. J Mater Sci: Mater Electron 28:3535–3541

Gao J, Hu M, Dong Y, Li RK (2013) Graphite-nanoplatelet-decorated polymer nanofiber with improved thermal, electrical, and mechanical properties. ACS Appl Mater Interfaces 5:7758–7764

Gong S, Schwalb W, Wang Y, Chen Y, Tang Y, Si J, Shirinzadeh B, Cheng W (2014) A wearable and highly sensitive pressure sensor with ultrathin gold nanowires. Nat Commun 5:3132

Hao T, Sun J, Wang W, Yu D (2018) MWCNTs-COOH/cotton flexible supercapacitor electrode prepared by improvement one-time dipping and carbonization method. Cellulose 25:4031–4041

He W, Li G, Zhang S, Wei Y, Wang J, Li Q, Zhang X (2015) Polypyrrole/silver coaxial nanowire aero-sponges for temperature-independent stress sensing and stress-triggered joule heating. ACS Nano 9:4244–4251

Kim D-H, Lu NS, Ma R, Kim Y-S, Kim R-H, Wang SD, Wu J, Won SM, Tao H, Islam A (2011) Epidermal electronics. Science 333:838–843

Konwar A, Baruah U, Deka MJ, Hussain AA, Haque SR, Pal AR, Chowdhury D (2017) Tea-carbon dots-reduced graphene oxide: an efficient conducting coating material for fabrication of an E-textile. ACS Sustain Chem Eng 5:11645–11651

Lee J, Kwon H, Seo J, Shin S, Koo JH, Pang C, Son S, Kim JH, Jang YH, Kim DE (2015) Conductive fiber-based ultrasensitive textile pressure sensor for wearable electronics. Adv Mater 27:2433–2439

Li Y, Hu YS, Titirici MM, Chen L, Huang X (2016) Hard carbon microtubes made from renewable cotton as high-performance anode material for sodium-ion batteries. Adv Energy Mater 6:1600659

Liang Y, Xiao P, Wang S, Shi J, He J, Zhang J, Huang Y, Chen T (2018) Scalable fabrication of free-standing, stretchable CNT/TPE ultrathin composite films for skin adhesive epidermal electronics. J Mater Chem C 6:6666–6671

Lin D, Zeng X, Li H, Lai X (2018) Facile fabrication of superhydrophobic and flame-retardant coatings on cotton fabrics via layer-by-layer assembly. Cellulose 25:3135–3149

Liu M, Pu X, Jiang C, Liu T, Huang X, Chen L, Du C, Sun J, Hu W, Wang ZL (2017) Large-area all-textile pressure sensors for monitoring human motion and physiological signals. Adv Mater 29:1703700

Liu W, Liu N, Yue Y, Rao J, Cheng F, Su J, Liu Z, Gao Y (2018) Piezoresistive pressure sensor based on synergistical innerconnect polyvinyl alcohol nanowires/wrinkled graphene film. Small 14:1704149

Lou Z, Chen S, Wang L, Jiang K, Shen G (2016) An ultra-sensitive and rapid response speed graphene pressure sensors for electronic skin and health monitoring. Nano Energy 23:7–14

Lou Z, Li L, Wang L, Shen G (2017) Recent progress of self-powered sensing systems for wearable electronics. Small 13:1701791

Ma Z, Wei A, Ma J, Shao L, Jiang H, Dong D, Ji Z, Wang Q, Kang S (2018) Lightweight, compressible and electrically conductive polyurethane sponges coated with synergistic multiwalled carbon nanotubes and graphene for piezoresistive sensors. Nanoscale 10:7116–7126

Pang C, Lee G-Y, T-i Kim, Kim SM, Kim HN, Ahn S-H, Suh K-Y (2012) A flexible and highly sensitive strain-gauge sensor using reversible interlocking of nanofibres. Nat Mater 11:795–801

Park J, Lee Y, Hong J, Ha M, Jung Y-D, Lim H, Kim SY, Ko H (2014) Giant tunneling piezoresistance of composite elastomers with interlocked microdome arrays for ultrasensitive and multimodal electronic skins. ACS Nano 8:4689–4697

Park H, Jeong YR, Yun J, Hong SY, Jin S, Lee S-J, Zi G, Ha JS (2015) Stretchable array of highly sensitive pressure sensors consisting of polyaniline nanofibers and Au-coated polydimethylsiloxane micropillars. ACS Nano 9:9974–9985

Su X, Li H, Lai X, Zhang L, Liang T, Feng Y, Zeng X (2017) Polydimethylsiloxane-based superhydrophobic surfaces on steel substrate: fabrication, reversibly extreme wettability and oil-water separation. ACS Appl Mater Interfaces 9:3131–3141

Su X, Li H, Lai X, Yang Z, Chen Z, Wu W, Zeng X (2018) Vacuum-assisted layer-by-layer superhydrophobic carbon nanotube films with electrothermal and photothermal effects for deicing and controllable manipulation. J. Mater. Chem. A 6:16910–16919

Tao L-Q, Zhang K-N, Tian H, Liu Y, Wang D-Y, Chen Y-Q, Yang Y, Ren T-L (2017) Graphene-paper pressure sensor for detecting human motions. ACS Nano 11:8790–8795

Viry L, Levi A, Totaro M, Mondini A, Mattoli V, Mazzolai B, Beccai L (2014) Flexible three-axial force sensor for soft and highly sensitive artificial touch. Adv Mater 26:2659–2664

Wan P, Yin S, Liu L, Li Y, Liu Y, Wang X, Leow W, Ma B, Chen X (2014) Graphene carrier for magneto-controllable bioelectrocatalysis. Small 10:647–652

Wang J, Jiu J, Nogi M, Sugahara T, Nagao S, Koga H, He P, Suganuma K (2015) A highly sensitive and flexible pressure sensor with electrodes and elastomeric interlayer containing silver nanowires. Nanoscale 7:2926–2932

Wang Q, Jian M, Wang C, Zhang Y (2017) Carbonized silk nanofiber membrane for transparent and sensitive electronic skin. Adv Funct Mater 27:1605657

Wang Y, Hao J, Huang Z, Zheng G, Dai K, Liu C, Shen C (2018) Flexible electrically resistive-type strain sensors based on reduced graphene oxide-decorated electrospun polymer fibrous mats for human motion monitoring. Carbon 126:360–371

Wei Y, Chen S, Li F, Lin Y, Zhang Y, Liu L (2015) Highly stable and sensitive paper-based bending sensor using

silver nanowires/layered double hydroxides hybrids. ACS Appl Mater Interfaces 7:14182–14191

Wei Y, Chen S, Lin Y, Yuan X, Liu L (2016) Silver nanowires coated on cotton for flexible pressure sensors. J Mater Chem C 4:935–943

Wu X, Han Y, Zhang X, Zhou Z, Lu C (2016) Large-area compliant, low-cost, and versatile pressure-sensing platform based on microcrack-designed carbon black@-polyurethane sponge for human-machine interfacing. Adv Funct Mater 26:6246–6256

Xia S, Song S, Gao G (2018) Robust and flexible strain sensors based on dual physically cross-linked double network hydrogels for monitoring human-motion. Chem Eng J 354:817–824

Xiang L, Zhang H, Hu Y, Peng L-M (2018) Carbon nanotube-based flexible electronics. J Mater Chem C 6:7714–7727

Xu X, Wang R, Nie P, Cheng Y, Lu X, Shi L, Sun J (2017) Copper nanowire-based aerogel with tunable pore structure and its application as flexible pressure sensor. ACS Appl Mater Interfaces 9:14273–14280

Yang C, Li L, Zhao J, Wang J, Xie J, Cao Y, Xue M, Lu C (2018a) Highly sensitive wearable pressure sensors based on three-scale nested wrinkling microstructures of poly-pyrrole films. ACS Appl Mater Interfaces 10:25811–25818

Yang Z, Pang Y, X-l Han, Yang Y, Ling J, Jian M, Zhang Y, Yang Y, Ren T-L (2018b) Graphene textile strain sensor with negative resistance variation for human motion detection. ACS Nano 12:9134–9141

Zhang M, Wang C, Wang H, Jian M, Hao X, Zhang Y (2017) Carbonized cotton fabric for high-performance wearable strain sensors. Adv Funct Mater 27:1604795

Zhao H, Kwak JH, Zhang ZC, Brown HM, Arey BW, Holladay JE (2007) Studying cellulose fiber structure by SEM, XRD, NMR and acid hydrolysis. Carbohydr Polym 68:235–241

Zhong W, Liu Q, Wu Y, Wang Y, Qing X, Li M, Liu K, Wang W, Wang D (2016) A nanofiber based artificial electronic skin with high pressure sensitivity and 3D conformability. Nanoscale 8:12105–12112